

**Modeling the fusion process with a modified Woods-Saxon potential in  $^{40}\text{Ar}$ -induced fusion reactions**

H. B. Zhou (周厚兵),<sup>1,2</sup> Z. Y. Li (李子晔) <sup>1</sup>, Z. G. Gan (甘再国),<sup>3</sup> Z. Y. Zhang (张志远),<sup>3</sup> H. Yao (姚红) <sup>4</sup>,  
 N. Wang (王宁),<sup>1,2,\*</sup> H. B. Yang (杨华彬),<sup>3</sup> L. Ma (马龙),<sup>3</sup> M. H. Huang (黄明辉),<sup>3</sup> C. L. Yang (杨春莉),<sup>3</sup>  
 M. M. Zhang (张明明),<sup>3</sup> Y. L. Tian (田玉林),<sup>3</sup> Y. S. Wang (王永生),<sup>3</sup> X. H. Zhou (周小红),<sup>3</sup> and J. L. Tian (田俊龙) <sup>5</sup>

<sup>1</sup>Department of Physics, Guangxi Normal University, Guilin 541004, People's Republic of China

<sup>2</sup>Guangxi Key Laboratory of Nuclear Physics and Technology, Guilin 541004, People's Republic of China

<sup>3</sup>CAS Key Laboratory of High Precision Nuclear Spectroscopy, Institute of Modern Physics, Chinese Academy of Sciences, Lanzhou 730000, China

<sup>4</sup>School of Physics, Beihang University, Beijing 102206, People's Republic of China

<sup>5</sup>School of Physics and Electrical Engineering, Anyang Normal University, Anyang 455000, People's Republic of China



(Received 5 December 2021; accepted 15 February 2022; published 28 February 2022)

The evaporation cross sections in fusion reactions by  $^{40}\text{Ar}$  bombarding deformed nuclei were compared to calculations using a modified Woods-Saxon potential model together with the standard statistical model. The results show that the predictions overestimate the experimental yields of these reaction products up to two orders of magnitude as the charge number of compound nuclei ( $Z_{CN} \geq 85$ ) increases, and suggest that the fusion process strongly depends on the orientation of the deformed target according to density-constrained time-dependent Hartree-Fock calculations.

DOI: [10.1103/PhysRevC.105.024328](https://doi.org/10.1103/PhysRevC.105.024328)

## I. INTRODUCTION

One of the most efficient methods to produce neutron-deficient isotopes above lead is to use heavy-ion induced fusion-evaporation reactions [1–3]. However, due to the low fission barriers and high excitation energies of the compound nuclei, the production cross sections for the formation of nuclei with  $N \approx 126$  would reach down to nanobarn levels or even less [4–6]. Therefore, a model that can self-consistently describe the processes of fusion reactions plays a vital role in choosing the optimum target-projectile-energy combinations in order to explore the unknown territories in the chart of nuclides, especially for the superheavy region.

An analytical method, named the modified Woods-Saxon (MWS) potential model, proposed by Wang *et al.* [7,8], has been developed to describe the entrance channel fusion barrier and the fission barrier of fusion-fission reactions. In this model, because one does not need to deal with the complex process of the calculations for the microscopic densities of the interacting nuclei, it is convenient for practical application. With the analytical MWS potential incorporating the statistical model HIVAP [9,10], a series of fusion excitation functions, such as those of  $^7\text{Li}$ -,  $^{12}\text{C}$ -, and  $^{16}\text{O}$ -induced fusion reactions [7], are reasonably well reproduced by the calculated results, while the calculations for heavy systems with  $^{208}\text{Pb}$  target present a significant deviation from the experimental data (see Fig. 13 in [7]). In this paper, we aim at testing the application

of the MWS potential model to the  $^{40}\text{Ar}$ -induced fusion reactions, and making a quantitative comparison between the theoretical predictions and the experimental observations.

## II. EXPERIMENTS

The cross sections of evaporation residues (ERs) were measured via reactions with  $^{40}\text{Ar}$  bombarding a Hf target (isotopically enriched 84.6%  $^{176}\text{Hf}$ , 8.94%  $^{177}\text{Hf}$ , 3.05%  $^{178}\text{Hf}$ , 1.16%  $^{179}\text{Hf}$ , and 2.23%  $^{180}\text{Hf}$ ). The  $^{40}\text{Ar}$  beams with energies of 183 and 190 MeV were delivered by the Sector-Focusing Cyclotron (SFC) of the Heavy Ion Research Facility in Lanzhou (HIRFL), China. The average beam intensity on target was about 500 pA. The targets with a thickness of  $410 \mu\text{g}/\text{cm}^2$  were prepared by sputtering the material onto  $40\text{-}\mu\text{g}/\text{cm}^2$ -thick carbon foils and then covered by  $10\text{-}\mu\text{g}/\text{cm}^2$ -thick carbon layer. The recoil ERs were separated by the gas-filled recoil separator SHANS [11] with a transport efficiency of  $\approx 14\%$  and collected by three 16-strip position-sensitive silicon detectors (PSSDs), which were mounted side by side at the focal plane of the separator. The active area of each PSSD is  $50 \times 50 \text{ mm}^2$ . The total detection efficiency for the full-energy  $\alpha$  particles emitted from ERs was measured to be  $\approx 54\%$ .  $\alpha$  particles escaping from the PSSDs were detected by eight side silicon detectors (SSDs) mounted perpendicular to the surface of PSSDs with an extra detection efficiency of  $\approx 18\%$ . The escape events were reconstructed by adding the registered energies in PSSDs and SSDs. Energy resolutions of PSSDs were about 45 keV (full width at half maximum) for 6.5–10.5 MeV  $\alpha$  particles. In order to distinguish the decay events from the implantation products, two multiwire proportional counters were mounted upstream from the PSSDs. A

\*Corresponding author: wangning@gxnu.edu.cn

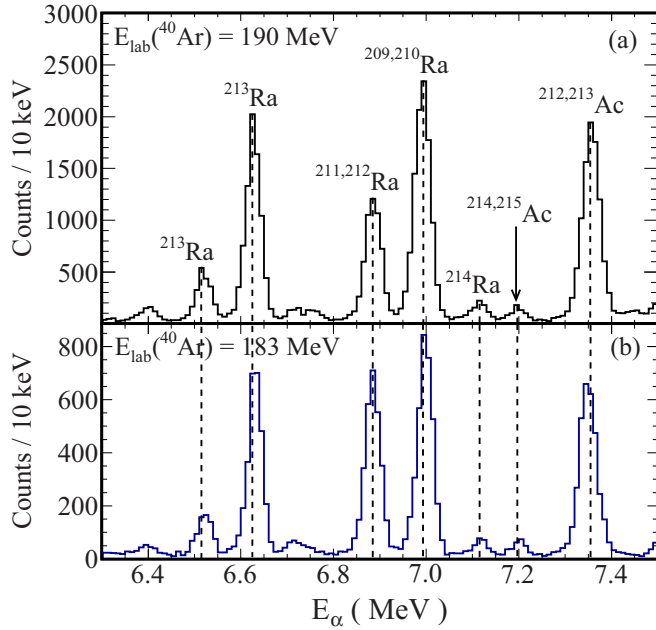


FIG. 1.  $\alpha$  spectra of evaporation residues produced in the reactions with  $^{40}\text{Ar}$  bombarding on Hf target at beam energies of (a) 190 MeV and (b) 183 MeV. Maximum searching time for the ER- $\alpha$  pairs is 25 s.

digital pulse readout technique was employed to record the signals in the experiment. Detailed descriptions of experiment setup and technique can be obtained in Refs. [12–15].

The identification of ERs was performed by ER- $\alpha$  correlation measurement. The  $\alpha$  spectra detected for three hours at different beam energies are presented in Fig. 1. The searching time window was set to be  $\Delta t(\text{ER}-\alpha) < 25$  s, which includes almost all the  $\alpha$  decay events from  $^{209,210}\text{Ra}$ . Due to the odd-even staggering in  $\alpha$ -decay energies, the  $\alpha$ -decay peaks of  $^{209,210}\text{Ra}$ ,  $^{211,212}\text{Ra}$ ,  $^{212,213}\text{Ac}$ , and  $^{214,215}\text{Ac}$  cannot be separated individually. The isotopes  $^{209,210}\text{Ra}$  and  $^{212,213}\text{Ac}$  were mainly produced via the reaction  $^{40}\text{Ar} + ^{176}\text{Hf}$ , while the isotopes  $^{211-214}\text{Ra}$  and  $^{214,215}\text{Ac}$  may be produced via the reactions of  $^{40}\text{Ar}$  with one or more Hf isotopes contained in the target material. In following, the production cross sections for  $^{209,210}\text{Ra}$  and  $^{212,213}\text{Ac}$  will be extracted and compared with the theoretical calculations.

### III. RESULTS AND DISCUSSION

With the information of the target thickness, beam intensity, detection efficiency, and transport efficiency of SHANS, the evaporation residue cross sections can be extracted by using the statistics of the characteristic  $\alpha$  particles presented in Fig. 1. The measured values for  $^{209,210}\text{Ra}$  and  $^{212,213}\text{Ac}$  at 183 and 190 MeV beam energies are listed in Table I. Only the statistical errors were considered. As reported in Ref. [7], the ER cross section is obtained with  $\sigma_{ER}(E_{c.m.}) = \sigma_{\text{cap}}(E_{c.m.})P_{CN}(E_{c.m.})W_{\text{sur}}(E_{c.m.})$ , where  $\sigma_{\text{cap}}$ ,  $P_{CN}$ , and  $W_{\text{sur}}$  are the capture cross section, the probability of the compound nucleus formation after the capture, and the survival probability of the excited compound nucleus, respectively. In this

TABLE I. Measured evaporation residue cross sections in this study. The errors represent statistical uncertainties only. The calculated values are listed in the last column.

Channel	$E_{\text{lab}}$ (MeV)	$\sigma_{\text{exp.}}$ ( $\mu\text{b}$ )	$\sigma_{\text{calc.}}$ ( $\mu\text{b}$ )
$^{176}\text{Hf}(^{40}\text{Ar}, p2n-3n)^{212,213}\text{Ac}$	183	1.31(2)	399
	190	4.67(5)	267
$^{176}\text{Hf}(^{40}\text{Ar}, \alpha 2n-3n)^{209,210}\text{Ra}$	183	1.41(2)	466
	190	5.15(5)	374

work, we neglect the influence of quasifission and thereby set  $P_{CN} = 1$ , for which the reason is given later. The capture cross sections  $\sigma_{\text{cap}}$  of the measured reactions were calculated within the framework of the MWS potential model, and the survival probabilities  $W_{\text{sur}}$  of the compound nuclei were obtained by using the statistical model HIVAP. Details of the model were described in Refs. [7, 16, 17]. The calculated values are shown in column 4 of Table I. It is found that the theoretical results are roughly two orders of magnitude larger than the experimental values.

A series of the measured cross sections in  $^{40}\text{Ar}$ -induced fusion reactions with isotopes of Ho, Tm, Yb, Lu, Hf, and Ta were reported in Ref. [4]. Theoretical calculations using the method as mentioned above were also performed for the same reaction systems in the present work. Some of the evaporation channels are shown in Fig. 2 for illustration. It is seen that the deviations between the experimental data and the theoretical predictions are increased significantly with the increase of the compound-nuclear charge number  $Z_{CN}$ .

To make a quantitative comparison between the experimental data and the calculations, the theory evaluation factor (TEF) [18] was introduced. The average TEF is defined as

$$\overline{\text{TEF}} = \frac{1}{N} \sum_i \log_{10} \left( \frac{\sigma_{th}^i}{\sigma_{exp}^i} \right). \quad (1)$$

Here  $N$  denotes the number of data points.  $\sigma_{th}$  and  $\sigma_{exp}$  denote the calculated and measured cross sections, respectively. The variance of the average TEF is calculated by

$$\Delta = \frac{1}{N} \left( \sum_i (\text{TEF}_i - \overline{\text{TEF}})^2 \right)^{1/2}. \quad (2)$$

It is worth noting that TEF is a logarithmic quantity. When theories have TEF values differing by 1 or 2, their reliabilities will actually differ by orders of magnitude.

The average theoretical evaluation factors for the  $^{40}\text{Ar}$ -induced reactions are shown in Fig. 3. For these systems, the MWS potential model gives a poor description of the data with the increase of the charge number of compound nuclei, and the deviation in terms of TEF implies a tendency of linear variation. In order to give an explanation of this phenomenon, we will discuss in the following how the fusion process depends on the deformation orientation [19–22] of the target with respect to the incident projectile.

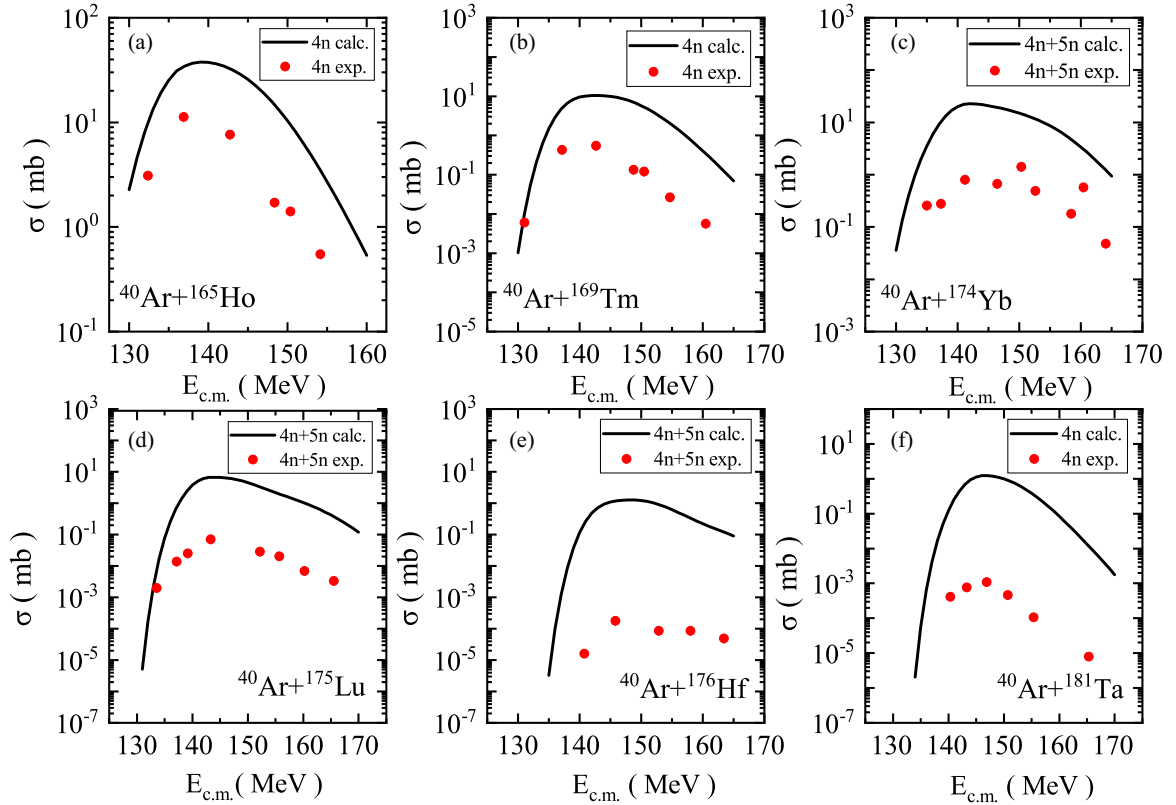


FIG. 2. Some of the evaporation residue cross sections in fusion reactions of  $^{40}\text{Ar}$  with isotopes of Ho, Tm, Yb, Lu, Hf, and Ta. The data were taken from Ref. [4].

To analyze the influence of quasifission, we present the nucleus-nucleus potential for the  $^{40}\text{Ar}$ -induced fusion reactions and the reaction  $^{48}\text{Ca} + ^{208}\text{Pb}$  obtained with the MWS potential in Fig. 4. It is found that the depths of the capture pockets, which are defined as the heights of the quasifission barriers in Ref. [16], for the former systems and the latter are 12 and 10 MeV, respectively. As discussed in Ref. [7], the

experimental data of the ER cross sections for the reaction  $^{48}\text{Ca} + ^{208}\text{Pb}$  were reasonably well reproduced at energies near and above the fission barrier without taking into account the influences of quasifission.

In addition, to check the depth of the capture pocket and the barrier height, we also study the fusion reaction  $^{40}\text{Ar} + ^{176}\text{Hf}$  with the time dependent Hartree-Fock theory. The nucleus-nucleus interaction potential is extracted by using the density-constrained time-dependent Hartree-Fock

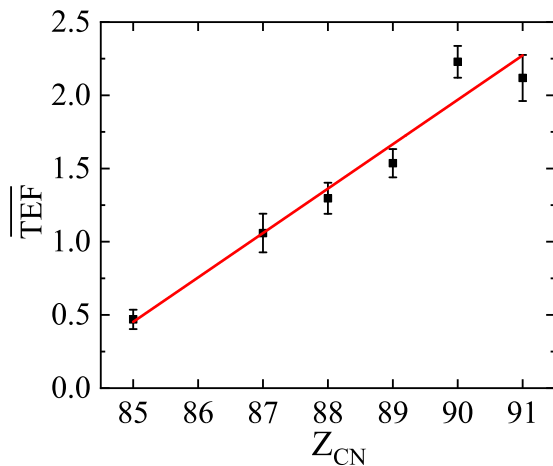


FIG. 3. Theory evaluation factors for  $^{40}\text{Ar}$ -induced fusion reactions using the modified Woods-Saxon potential model. The experimental data are taken from Ref. [4] and this work. The solid line is obtained by linear fitting.

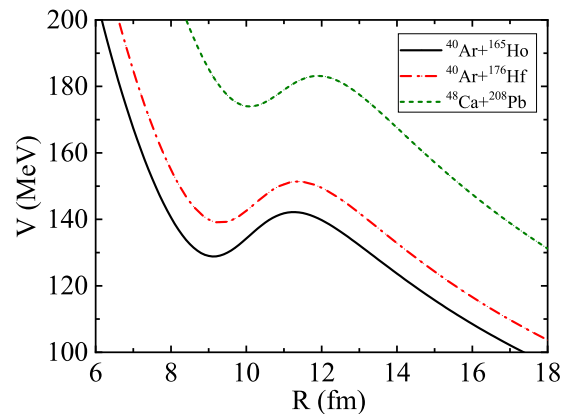


FIG. 4. Nucleus-nucleus potentials for fusion reactions of  $^{40}\text{Ar}$  with isotopes of  $^{165}\text{Ho}$  and  $^{176}\text{Hf}$  obtained with the modified Woods-Saxon potential. The potential barrier for  $^{48}\text{Ca} + ^{208}\text{Pb}$  is also presented for comparison.

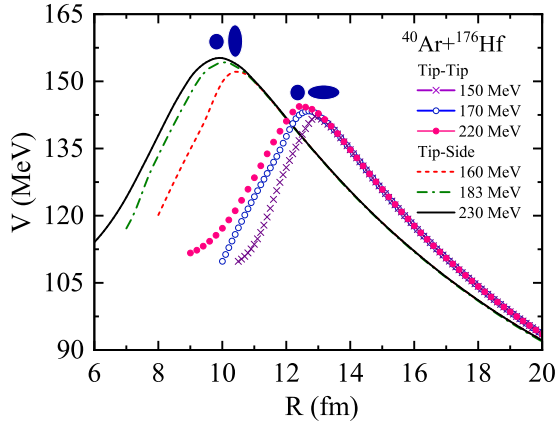


FIG. 5. Fusion potential for reaction  $^{40}\text{Ar} + ^{176}\text{Hf}$  from the density-constrained time-dependent Hartree-Fock calculations at different center-of-mass energies.

(DC-TDHF) approach [23–25] at tip-tip and tip-side orientations considering the deformation of the targets. In this method, the incident energies at the center of mass are taken as  $\approx 0.99$  times and  $\approx 1.05$  times the MWS barrier, respectively. The Skyrme SLy4d interactions [26] are used by static HF and TDHF dynamic evolution, in which the numerical boxes are chosen as  $30 \times 30 \times 30 \text{ fm}^3$  and  $30 \times 30 \times 50 \text{ fm}^3$ , respectively. The time propagation is carried out using a Talyor-series expansion up to the sixth order of the unitary mean-field propagator with a time step of  $0.2 \text{ fm}/c$ , and the initial distance of two nuclei is set to 20 fm. The capture cross section at different energies can be calculated by using the transmission matrix [27] with the nucleus-nucleus interaction potential extracted by DC-TDHF. For brevity, only the reaction  $^{40}\text{Ar} + ^{176}\text{Hf}$  is shown in Fig. 5. One can see that the calculated depths of capture pockets in this system are larger than 20 MeV for both the tip-tip and tip-side collisions, which also indicates that the quasifission is unlikely to occur. Thus, it is reasonable to set  $P_{CN} = 1$  in the present work.

In Fig. 6, we show the capture cross sections obtained with the MWS potential model and those with the DC-TDHF approach. In the TDHF calculations, we consider the different orientations of the projectile and target nuclei in the collisions. The dashed black curve denotes the calculated capture cross sections based on the nucleus-nucleus potential from the TDHF theory at tip-tip orientation. The dotted green curve denotes the corresponding results at tip-side orientation. One can see that the descriptions of the fusion processes using the two methods agree well with each other at energies above the barrier for the reaction  $^{40}\text{Ar} + ^{176}\text{Hf}$ . However, a significant difference is observed near and below the barrier, and the capture cross sections given by the DC-TDHF approach present an obvious dependence on the orientation of the deformed target nucleus at the collision point. With the DC-TDHF approach together with the HIVAP model, we estimated the upper and lower limits of the  $1p2n + 1p3n$  and  $\alpha 2n + \alpha 3n$  cross sections (see the shaded areas in Fig. 6). The experimental data are also presented for comparison. It is found that the experimental data from our work and Ref. [4] can be reproduced at energies near the fusion barrier. The low yields of the

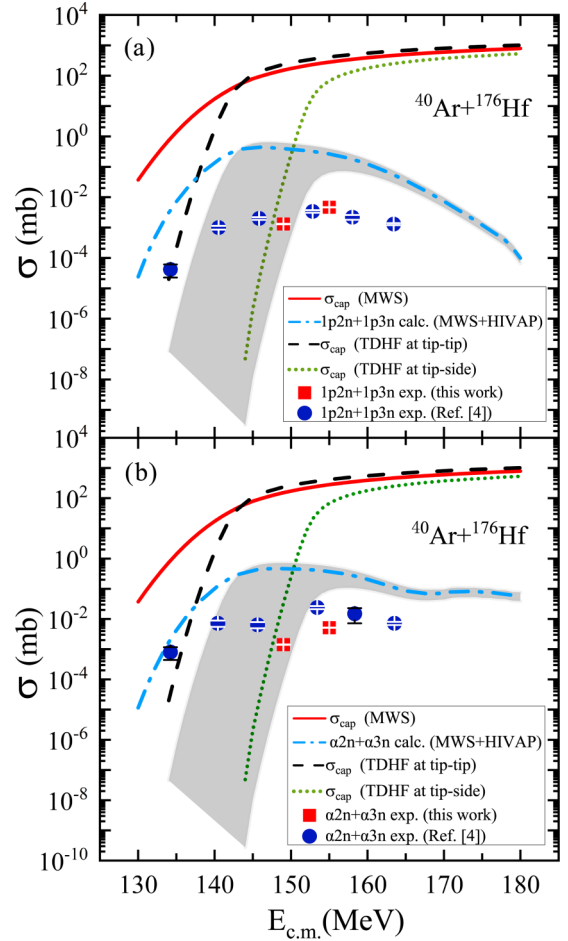


FIG. 6. Cross sections of reaction  $^{40}\text{Ar} + ^{176}\text{Hf}$ .  $\sigma_{\text{cap}}$  denotes the capture cross section. The incident energies at the center of mass are taken as 150 and 160 MeV to calculate the fusion barriers for the tip-tip collision and the tip-side collision by using the DC-TDHF method, respectively. The shaded areas in (a) and (b) denote the cross sections of  $1p2n + 1p3n$  and  $\alpha 2n + \alpha 3n$  channels obtained with the DC-TDHF+HIVAP method, respectively.

evaporation residue measured in the experiment imply that the tip-side collision is favorable in this reaction system. At very low incident energy ( $E_{c.m.} \approx 134 \text{ MeV}$  [4]), one should note that the experimental datum seems to be in better agreement with the prediction given by the MWS+HIVAP method. This phenomenon indicates that a unified description of the fusion processes is still a challenge for this reaction. The deviations above the barrier may be originating from the influences of the compound-nuclear fission. The dependence of the survival probability  $W_{\text{sur}}$  on the fission barrier was tested during the calculations. For the compound nucleus  $^{216}\text{Th}$  produced by the reaction  $^{40}\text{Ar} + ^{176}\text{Hf}$ , as an example, the fission barrier obtained with the MWS potential and incorporating the shell correction [7] is 8.63 MeV, which is very close to the value of 8.27 MeV obtained with GEF model [28], but it is smaller than the value of 12.17 MeV given by Möller's [29] method. Through varying the barrier height by about 2 MeV, the survival probability obtained from the HIVAP model will roughly

differ by an order of magnitude. On the other hand, as presented in Fig. 3, a more reliable prediction would be obtained by multiplying the calculated value by a constant ratio, which is helpful for choosing the optimum target-projectile-energy combinations in the experiment.

#### IV. SUMMARY

The cross sections of  $^{209,210}\text{Ra}$  and  $^{212,213}\text{Ac}$  were measured by the reaction  $^{40}\text{Ar} + ^{176}\text{Hf}$  with the help of SHANS at HIRFL. The results show that the experimental data are much smaller than the predictions obtained from the MWS potential together with HIVAP model. The theory evaluation factors were extracted to make a quantitative comparison between the calculations and the observations in  $^{40}\text{Ar}$ -induced

fusion reactions. It is found that the deviations between theories and experiments increase by orders of magnitude over the compound-nuclear charge number. Combined with DC-TDHF calculations, we suggest that the influences of deformation orientation should be taken into account in the fusion processes.

#### ACKNOWLEDGMENTS

The authors thank the accelerator staff of HIRFL for providing the stable  $^{40}\text{Ar}$  beam. This work was supported by the National Natural Science Foundation of China (Grants No. 11965003, No. 11505035, No. U1867212) and the Natural Science Foundation of Guangxi (Grants No. 2017GXNS-FAA198160, No. 2017GXNSFGA198001).

- 
- [1] M. Thoennessen, *The Discovery of Isotopes: A Complete Compilation* (Springer, Heidelberg, 2016).
- [2] V. I. Zagrebaev, *Phys. Rev. C* **64**, 034606 (2001).
- [3] Z. Feng, G. Jin, F. Fu, and J. Li, *Nucl. Phys. A* **771**, 50 (2006).
- [4] D. Vermeulen, H. G. Clerc, C. C. Sahm *et al.*, *Z. Phys. A: At. Nucl.* **318**, 157 (1984).
- [5] Z. Y. Zhang, H. B. Yang, M. H. Huang, Z. G. Gan, C. X. Yuan, C. Qi, A. N. Andreyev, M. L. Liu, L. Ma, M. M. Zhang, Y. L. Tian, Y. S. Wang, J. G. Wang, C. L. Yang, G. S. Li, Y. H. Qiang, W. Q. Yang, R. F. Chen, H. B. Zhang, Z. W. Lu *et al.*, *Phys. Rev. Lett.* **126**, 152502 (2021).
- [6] Z. Y. Zhang, Z. G. Gan, H. B. Yang, L. Ma, M. H. Huang, C. L. Yang, M. M. Zhang, Y. L. Tian, Y. S. Wang, M. D. Sun, H. Y. Lu, W. Q. Zhang, H. B. Zhou, X. Wang, C. G. Wu, L. M. Duan, W. X. Huang, Z. Liu, Z. Z. Ren, S. G. Zhou *et al.*, *Phys. Rev. Lett.* **122**, 192503 (2019).
- [7] N. Wang, K. Zhao, W. Scheid, and X. Wu, *Phys. Rev. C* **77**, 014603 (2008).
- [8] M. Liu, N. Wang, Z. X. Li *et al.*, *Nucl. Phys. A* **768**, 80 (2006).
- [9] S. Hofmann, V. Ninov, F. P. Heßberger *et al.*, *Z. Phys. A* **350**, 277 (1995).
- [10] W. Reisdorf, *Z. Phys. A* **300**, 227 (1981).
- [11] Z. Y. Zhang, L. Ma, Z. G. Gan *et al.*, *Nucl. Instrum. Methods Phys. Res., B* **317**, 315 (2013).
- [12] H. B. Zhou, Z. G. Gan, N. Wang, H. B. Yang, L. Ma, M. H. Huang, C. L. Yang, M. M. Zhang, Y. L. Tian, Y. S. Wang, Z. Y. Li, C. X. Yuan, S. Huang, X. J. Sun, H. Y. Peng, L. Ou, and X. H. Zhou, *Phys. Rev. C* **103**, 044314 (2021).
- [13] M. M. Zhang, H. B. Yang, Z. G. Gan *et al.*, *Phys. Lett. B* **800**, 135102 (2020).
- [14] L. Ma, Z. Y. Zhang, Z. G. Gan, X. H. Zhou, H. B. Yang, M. H. Huang, C. L. Yang, M. M. Zhang, Y. L. Tian, Y. S. Wang, H. B. Zhou, X. T. He, Y. C. Mao, W. Hua, L. M. Duan, W. X. Huang, Z. Liu, X. X. Xu, Z. Z. Ren, S. G. Zhou, and H. S. Xu, *Phys. Rev. Lett.* **125**, 032502 (2020).
- [15] H. B. Yang, Z. G. Gan, Z. Y. Zhang, M. M. Zhang, M. H. Huang, L. Ma, and C. L. Yang, *Eur. Phys. J. A* **55**, 8 (2019).
- [16] N. Wang, J. L. Tian, and W. Scheid, *Phys. Rev. C* **84**, 061601(R) (2011).
- [17] N. Wang, Z. X. Li, and W. Scheid, *J. Phys. G: Nucl. Part. Phys.* **34**, 1935 (2007).
- [18] J. S. Barrett, W. Loveland, R. Yanez, S. Zhu, A. D. Ayangeakaa, M. P. Carpenter, J. P. Greene, R. V. F. Janssens, T. Lauritsen, E. A. McCutchan, A. A. Sonzogni, C. J. Chiara, J. L. Harker, and W. B. Walters, *Phys. Rev. C* **91**, 064615 (2015).
- [19] R. G. Stokstad, Y. Eisen, S. Kaplanis, D. Pelte, U. Smilansky, and I. Tseruya, *Phys. Rev. Lett.* **41**, 465 (1978).
- [20] C. R. Morton, A. C. Berriman, R. D. Butt, M. Dasgupta, D. J. Hinde, A. Godley, J. O. Newton, and K. Hagino, *Phys. Rev. C* **64**, 034604 (2001).
- [21] S. Mitsuoka, H. Ikezoe, K. Nishio, K. Satou, and J. Lu, *Phys. Rev. C* **65**, 054608 (2002).
- [22] V. Yu. Denisov and N. A. Pilipenko, *Phys. Rev. C* **81**, 025805 (2010).
- [23] A. S. Umar, V. E. Oberacker, R. Keser *et al.*, in *Nuclear Structure and Dynamics 2012*, 9–13 July 2012, Opatija, Croatia, T. Nikšić, M. Milin, D. Vretenar, and S. Szilner, AIP Conf. Proc. No. 1491 (AIP, New York, 2012), p. 369.
- [24] A. S. Umar and V. E. Oberacker, *Phys. Rev. C* **74**, 021601(R) (2006).
- [25] A. S. Umar, V. E. Oberacker, J. A. Maruhn, and P. G. Reinhard, *Phys. Rev. C* **80**, 041601(R) (2009).
- [26] K.-H. Kim, T. Otsuka, and P. Bonche, *J. Phys. G: Nucl. Part. Phys.* **23**, 1267 (1997).
- [27] Y. Qin, J. Tian, Y. Yang, and N. Wang, *Phys. Rev. C* **85**, 054623 (2012).
- [28] K. H. Schmidt, B. Jurado, C. Amouroux, and C. Schmitt, *Nucl. Data Sheets* **131**, 107 (2016).
- [29] P. Möller and J. Randrup, *Phys. Rev. C* **91**, 044316 (2015).